Research Square

Preprints are preliminary reports that have not undergone peer review.
They should not be considered conclusive, used to inform clinical practice,
or referenced by the media as validated information.

Effects of Low-Level Laser Therapy Versus Injectable Hyaluronic Acid Combined with Platelet-Rich Plasma on Orthodontic Tooth Movement

Hani AlSwafeeri

hani.alswafiri@pua.edu.eg

Pharos University in Alexandria

Wafaa Alghonemy

Tanta University

Rehab El Sharkawy

Pharos University in Alexandria

Rania Hanafy

Pharos University in Alexandria

Menna Beshara

Pharos University in Alexandria

Khaled AboulAzm

Pharos University in Alexandria

Eman Salem

Pharos University in Alexandria

Research Article

Keywords: Orthodontic tooth movement, low-level laser therapy, Hyaluronic acid nanoparticles, platelet rich plasma, periodontal ligament, alveolar bone

Posted Date: November 11th, 2026

DOI: https://doi.org/10.21203/rs.3.rs-11458776/v1

License: This work is licensed under a Creative Commons Attribution 4.0 International License.
Read Full License

Additional Declarations: No competing interests reported.

Effects of Low-Level Laser Therapy Versus Injectable Hyaluronic Acid Combined with Platelet-Rich Plasma on Orthodontic Tooth Movement

Hani AlSwafeeri[a*], Wafaa Yahia Alghonemy[b,c], Rehab El Sharkawy[d], Rania A. Hanafy [e], Menna Galal Beshara[f], Khaled AboulAzm[a], Eman M. Salem[g]

[a] Department of Orthodontics, Faculty of Dentistry, Pharos University in Alexandria, P.O. Box 37, Sidi Gaber, Alexandria, Egypt. hani.alswafiri@pua.edu.eg https://orcid.org/0000-0003-3848-2001

[b] Basic Dental Sciences Department, Faculty of Dentistry, Zarqa University, Zarqa, Jordan. PO Box 2000, Zarqa, 13110 Jordan.

[c] Oral Biology Department, Faculty of Dentistry, Tanta University, Tanta, Egypt. Email: Wafaa_yehya@dent.tanta.edu.eg. https://orcid.org/0000-0002-0452-2565.

[d] Chemistry Department, Faculty of Dentistry, Pharos University in Alexandria, P.O. Box 37, Sidi Gaber, Alexandria, Egypt, rehab.mansour@pua.edu.eg

[e] Dental Materials Department, Faculty of Dentistry, Pharos University in Alexandria, P.O. Box 37, Sidi Gaber, Alexandria, Egypt. rania.hanafy@pua.edu.eg.

[f] Faculty of Dentistry, Pharos University in Alexandria, P.O. Box 37, Sidi Gaber, Alexandria, Egypt. Mennagelal@icloud.com

[a]Department of Orthodontics, Faculty of Dentistry, Pharos University in Alexandria, P.O. Box 37, Sidi Gaber, Alexandria, Egypt. k.aboulazm@pua.edu.eg

[g] Oral Biology Department, Faculty of Dentistry, Pharos University in Alexandria, P.O. Box 37, Sidi Gaber, Alexandria, Egypt. eman.salem@pua.edu.eg. https://orcid.org/0000-0003-4464-8653.

***Corresponding author name and email address: Hani AlSwafeeri - hani.alswafiri@pua.edu.eg**

Running title: Accelerated Orthodontic Tooth Movement Using HA/PRP and Laser

Abstract:

Background: Accelerating orthodontic tooth movement (OTM) without compromising periodontal tissue integrity remains a substantial challenge in clinical orthodontics. Low-level laser therapy (LLLT) and biologic regenerative strategies have been explored to modulate periodontal tissue responses and alveolar bone remodeling. **Aim:** To compare the effects of LLLT and a mixture of hyaluronic acid nanoparticles (HA-NPs) and platelet-rich plasma (PRP) on OTM and the associated histological changes in periodontal and alveolar bone tissues in rabbits. **Methods:** Eighteen healthy adult male rabbits were divided into three groups: control, LLLT, and HA-NP/PRP. The LLLT group was irradiated with a 940-nm diode laser at six points around the maxillary incisors during orthodontic tooth movement. OTM and histological evaluations were assessed to evaluate periodontal ligament (PDL) width, osteoclast numbers, remodeled bone area, vascular area, and cellular activity. **Results:** Mean OTM was 1.12 ± 0.08 mm in the control, 1.29 ± 0.10 mm in the LLLT, and 1.37 ± 0.12 mm in the HA-NP/PRP. OTM was statistically greater in both intervention groups, but the overall OTM was not statistically significant ($p = 0.084$). Histological analysis showed significant differences between groups in PDL width ($p = 0.021$), osteoclast number ($p = 0.015$), and area of remodeled bone ($p = 0.008$), with the maximum values reported in the HA-NP/PRP. Vascular area and cellular activity increased in the control, LLLT, and HA-NP/PRP groups, which suggests differences in the periodontal tissue response of the experimental groups **Conclusion:** LLLT and HA-NP/PRP treatment were associated with histological changes compatible with periodontal tissue remodeling during OTM. However, these biological changes did not translate into a statistically significant difference in OTM. Additional studies with longer observational periods are required to elucidate the relationship between histological responses and OTM.

Keywords: Orthodontic tooth movement; low-level laser therapy; Hyaluronic acid nanoparticles; platelet rich plasma; periodontal ligament; alveolar bone.

1. Introduction

Orthodontic tooth movement (OTM) is a biologic process that occurs through remodeling of the alveolar bone and periodontal ligament (PDL) in response to the application of mechanical forces [1]. Although conventional orthodontic treatment is effective in correcting malocclusion and improving oral function and esthetics, the prolonged treatment period remains a major concern for both clinicians and patients[2]. Extended OTM time is frequently associated with several undesirable consequences, including gingival inflammation, enamel demineralization, dental caries, root resorption, and decreased patient compliance[3, 4]. Therefore, accelerating OTM while maintaining periodontal health has become an important objective in modern orthodontics. Various approaches have been proposed to accelerate OTM, including surgical interventions, pharmacological agents, mechanical stimulation, and physical modalities[5–7]. However, many invasive techniques may increase patient discomfort and postoperative complications. Consequently, recent research has focused on minimally invasive methods that enhance bone remodeling and cellular activity while reducing adverse effects[6].

Low-level laser therapy (LLLT) has received attention as a non-invasive adjunctive technique in orthodontics[8]. LLLT is believed to stimulate cellular metabolism, increase vascularization, and enhance osteoclastic and osteoblastic activity through photobiomodulation[8–10]. Several studies have demonstrated that diode lasers may accelerate bone remodeling and periodontal tissue turnover, potentially enhancing the rate of OTM[11, 12]. Nevertheless, the available literature remains controversial, as some investigations reported a significant acceleration of OTM, whereas others found limited or no clinical effect[13]. These inconsistent findings may be related to variations in laser wavelength, energy density, application protocols, and experimental models[14].

Recently, biologically active injectable materials have emerged as promising adjuncts for tissue regeneration and for modulating bone remodeling [15–18]. An autologous blood product with a high concentration of growth factors is called platelet-rich plasma, or PRP, including transforming growth factor-beta (TGF-β), platelet-derived growth factor (PDGF), , and vascular endothelial growth factor (VEGF), which are known to enhance formation new blood vessels, cellular proliferation, and tissue

restoration[18, 19]. PRP has demonstrated beneficial effects on periodontal regeneration and bone healing, and may accelerate OTM by stimulating osteoclastic activity and alveolar bone remodeling [20, 21].

Hyaluronic acid (HA) is a naturally occurring glycosaminoglycan that plays an essential role in extracellular matrix organization, tissue hydration, wound healing, and inflammatory modulation [22]. Within the PDL, HA contributes to cellular migration, proliferation, and tissue repair [23]. In addition, HA possesses anti-inflammatory and osteoconductive properties that may support periodontal remodeling during OTM [23]. Recent studies have suggested that combining HA with PRP may enhance the regenerative potential of both materials by improving growth factor release and prolonging their local retention at the site of application [22, 24].

Despite LLLT, PRP, and HA potentially enhancing tissue remodeling during OTM, no prior experimental study has evaluated the biological effects of LLLT versus HA nanoparticles combined with PRP in an orthodontic context. Therefore, the present study intended to compare the effects of LLLT and injectable HA nanoparticles combined with PRP on OTM in rabbits, via quantitative, histological, and histomorphometric assessments.

2. Materials and Methods

2.1. Ethical Acceptance

The research procedure was authorized by the Pharos University of Alexandria's Faculty of Dentistry Research Ethics Committee, Egypt. The institutional protocols for the care and use of laboratory animals were followed in all experimental methods, the ARRIVE 2.0 guidelines [25].

2.2. Sample Size

Sample size calculation was performed based on previously published experimental revisions evaluating accelerated OTM [26]. Adopting a power of 80% ($\beta\beta = 0.20$) to detect a standardized effect size in OTM (primary outcome) of 0.8140, and a significance level of 5% (accepted α error =0.05), the necessary sample size was considered to be 18 healthy adult male rabbits. These rabbits were included in the study and randomly allocated into three equal groups (n = 6) using a computer-generated

randomization method. Any specimen loss resulting from a processing error will be replaced to maintain the sample size [27].

2.3. Animal preparation and group assignment

Eighteen healthy adult (7-10 months) male New Zealand white rabbits weighing between 2 and 2.5 kg were employed. The experimental animals were bred at the Faculty of Agriculture, Alexandria University, Egypt, and were purchased from this institution. Following purchase, the animals were transferred to the animal house where they were housed under appropriate environmental and husbandry conditions throughout the experimental period. The animals displayed normal dentition and were free from systemic or oral diseases at baseline. They were housed individually in stainless steel cages under standardized laboratory conditions, with controlled temperature, humidity, and a 12-hour cycle of light and dark. All rabbits received a soft diet and water during the duration of the experiment. Before the experiment began, a two-week acclimatization period was permitted, as per protocols approved by the Institutional Animal Care and Use Committee (IACUC) [28].

The rabbits were randomly divided into the following:

1- Group I (+ve Control Group): OTM was applied without administration of LLLT or HA+PRP.

2- Group II (LLLT Group): OTM was applied with LLLT administration.

3- Group III (HA-NP/PRP Group): OTM was applied in addition to the injection of formulated HA-NP/PRP.

3.4. Materials

Pharmaceutical-grade hyaluronic acid (HA) powder (molecular weight approximately 150–300 kDa; Advent Co., India) was employed to synthesize the HA hydrogel. Calcium chloride dihydrate ($CaCl_2 \cdot 2H_2O$; molecular weight: 147.02 g/mol; assay ≥99.0%) was acquired from Sigma-Aldrich, USA. Sterile phosphate-buffered saline (PBS) and other analytical-grade reagents were obtained from commercial suppliers and used as received. Sterile syringes and centrifuge tubes were used for PRP preparation. Whole blood was drawn and placed in sterile tubes with an anticoagulant of 3.8% sodium citrate for PRP preparation, after the rabbits were humanely euthanized, with 3 animals used.

3.5. Instrumentation

The prepared samples were characterized using complementary spectroscopic and microscopic techniques to evaluate their chemical structure, surface morphology, and nanoscale characteristics. Fourier-transform infrared (FT-IR) spectroscopy was achieved using a BRUKER VERTEX 70 spectrophotometer (Bruker, Germany) over the wavenumber range of 400–4000 cm^{-1} to identify the characteristic functional groups and chemical bonds present in the samples. The surface morphology and microstructural features of the samples were examined using a scanning electron microscope (SEM; JSM-IT200, JEOL Ltd., Japan). Before SEM analysis, the samples were sputter-coated using a JEOL-JFC-1100E coating unit to provide a conductive surface and diminish charging effects during electron-beam irradiation. The SEM was operated in the appropriate imaging mode, and characteristic micrographs were obtained at suitable magnifications to assess the surface morphology and particle characteristics. The nanoscale morphology and particle dimensions were further studied using a JEOL JEM-1400 Plus transmission electron microscope (HR-TEM; JEOL Ltd., Japan). HR-TEM imaging was performed in the suitable imaging mode, and representative micrographs were acquired to assess particle morphology, dispersion, and approximate particle size. The HR-TEM analysis provided complementary nanoscale morphological information to that gained from SEM.

The particle size, polydispersity index (PDI), and zeta potential of the HA nanoparticle dispersion were determined using a Zetasizer Nano ZS (Malvern Instruments Ltd., Malvern, UK). Dynamic light scattering (DLS) was employed to determine the hydrodynamic particle size and PDI, whereas electrophoretic light scattering was used to measure the zeta potential. The HA nanoparticle dispersion was appropriately diluted with deionized water before analysis. Samples intended for particle-size and PDI measurements were transferred into square glass cuvettes, while zeta-potential measurements were performed using transparent disposable zeta cells. All measurements were performed in triplicate under identical experimental conditions. These measurements were conducted on the HA nanoparticle formulation before PRP incorporation, as PRP was incorporated immediately before administration, and the final HA–PRP formulation was not intended for long-term storage as a nanodispersion.

The rheological behavior and viscosity of the HA nanoparticle formulation were assessed by using a Brookfield DV-II+ Pro RV rotational viscometer (AMETEK Brookfield, Middleboro, MA, USA) equipped with an RV-3 spindle. Approximately 25 mL of the formulation was transferred into the measurement container, ensuring

appropriate spindle immersion. Measurements were carried out at a rotational speed of 20 rpm and a controlled temperature of 25 ± 0.5 °C. Viscosity measurements were obtained in triplicate and expressed in centipoise (cP). The viscosity measurements were implemented to assess the flow characteristics and injectability of the HA formulation through a fine-gauge needle.

3.6. Synthesis

3.6.1 Synthesis of Hyaluronic Acid Nanoparticles (HA)

HA nanoparticles were synthesized according to a previously reported method with minor modifications [29]. Briefly, HA was dissolved in distilled water at a concentration of 0.5% (w/v) under continuous magnetic stirring at 800 rpm and room temperature until a clear, homogeneous polymeric solution was obtained. Nanoparticle formation was achieved through ionic interactions between HA and calcium ions. Briefly, an aqueous solution of calcium chloride dihydrate ($CaCl_2 \cdot 2H_2O$) at 0.1% (w/v) was introduced dropwise to the HA solution under continuous magnetic stirring. The gradual addition of $CaCl_2 \cdot 2H_2O$ was performed to facilitate interactions between Ca^{2+} ions and the negatively charged carboxylate groups of the HA chains, promoting the formation of nanoscale HA aggregates. Following the complete addition of the $CaCl_2 \cdot 2H_2O$ solution, the suspension was continuously stirred for an additional 2 h at room temperature to develop further and stabilize the formed HA nanoparticles. The resulting nanoparticle suspension was subsequently purified by centrifugation at 12,000 rpm for 15 min. The supernatant was carefully removed, and the collected nanoparticle pellet was washed three times with sterile phosphate-buffered saline (PBS) to eliminate remaining unreacted HA and excess calcium ions. Following the final washing step, the purified HA nanoparticles were collected and freeze-dried to obtain a dry powder. The freeze-dried HA nanoparticles were stored under appropriate conditions until further characterization and integration into the activated PRP.

3.6.2 Synthesis of Platelet-Rich Plasma (PRP)

PRP was prepared using a double-spin centrifugation protocol, with alterations based on a previously reported procedure[22]. Whole blood was collected under sterile conditions into tubes containing 3.8% sodium citrate as an anticoagulant. The anticoagulated blood was initially centrifuged at 1000 rpm for 10 min to separate the cellular components from the plasma fraction. The upper plasma fraction containing

platelets was carefully transferred to sterile tubes and subjected to a second centrifugation at 2000 rpm for 10 min. Then, the upper platelet-poor plasma (PPP) fraction was carefully removed, while the lower platelet-enriched plasma fraction was retained. The platelet-containing fraction was gently resuspended to obtain the final PRP preparation. The freshly prepared PRP was used within 6 h of collection.

3.6.3 Activation of PRP

Immediately before incorporation with the HA nanoparticles, the freshly prepared PRP was activated using a 10% (w/v) $CaCl_2 \cdot 2H_2O$ solution. Briefly, 50 µL of the $CaCl_2 \cdot 2H_2O$ solution was added to 3 mL of freshly prepared PRP, then gently mixed to ensure uniform distribution of the activating agent. Based on the molar mass of $CaCl_2 \cdot 2H_2O$ (147.02 g/mol), the calculated final concentration of $CaCl_2$ in the PRP mixture was approximately 11.2 mM. The activated PRP was used immediately for incorporation with the HA nanoparticles and subsequent administration.

3.6.4. Synthesis of the HA-NP/Activated-PRP Formulation

The HA nanoparticle–PRP formulation was synthesized immediately before administration to ensure the use of freshly activated PRP. Based on a previously reported HA-enriched PRP preparation, 25 mg of HA was incorporated into 1.0 mL of activated PRP and gently mixed with light circular motions until a homogeneous formulation was obtained [30, 31]. In the present study, the reported approach was adapted by incorporating 25 mg of the freeze-dried HA nanoparticles into 1.0 mL of freshly activated PRP. The components were gently mixed until the nanoparticles were homogeneously incorporated throughout the PRP matrix. The resulting HA-NP/PRP formulation was prepared immediately before administration and used without prolonged storage. This approach is consistent with recent evidence supporting the feasibility of injectable combinations of PRP with non-crosslinked HA for local therapeutic applications.

3.7. Orthodontic Appliance Placement

All rabbits were anesthetized before appliance placement using an intramuscular combination of 2% xylazine (Adwia, 10th of Ramadan City, Egypt) and 10% ketamine hydrochloride (Ketamine Alfasan 10%, Woerden, The Netherlands), at dosages of 0.2 mL/kg and 0.5 mL/kg body weight, respectively[32]. Small retention notches were prepared on the labial surfaces of the maxillary incisors approximately

1.5–2 mm above the gingival margin using a small round bur under continuous saline irrigation **(Figure 1A&B).** OTM was induced using stainless steel orthodontic expansion springs with 10 mm arms, secured between the maxillary incisors, to deliver approximately 50 g of continuous orthodontic force throughout the experimental period **(Figure 1C&D).** The experimental period lasted for 14 days.

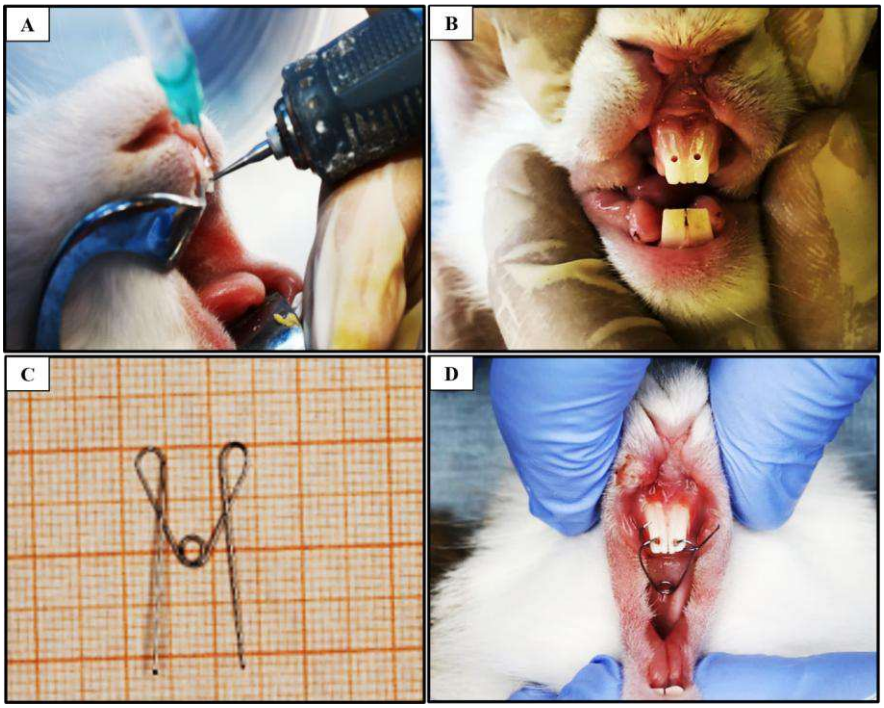


Figure 1. Experimental procedures of the orthodontic model. (A) Standardized perforation of the maxillary incisors using a low-speed dental handpiece. **(B)** Maxillary incisors after preparation of the standardized perforation sites. **(C)** An orthodontic spring is used in the study. **(D)** The placement and fixation of the orthodontic spring on the maxillary incisors.

3.8. LLLT Application Protocol

Rabbits in Group II received LLLT irradiation using a 940-nm diode laser **(Figure 2A)**. Laser application was performed at six points surrounding the maxillary incisors, with an output power of 0.1 W for 10 seconds per point in continuous mode **(Figure 2B&C).** LLLT irradiation was performed on days 1, 3, 8, and 10 following orthodontic appliance placements.



Figure 2. Application of LLLT. **(A)** Configuration of the 940-nm diode laser with an output power of 100 mW in continuous-wave mode. **(B)** Laser irradiation was delivered at six points surrounding the maxillary incisors for 10 s per point, corresponding to 1 J per point (6 J per session). **(C)** Three-dimensional illustration of the six LLLT application points (red dots) around the maxillary incisors in the rabbit orthodontic model.

3.9. Administration of Injectable HA-NP/PRP

Rabbits in Group III received local injections of the prepared injectable HA formulation mixed with PRP, approximately 0.5 mL[23], into the buccal mucosa adjacent to the moving teeth under sterile conditions at predetermined intervals during the experimental period.

3.10. Clinical Evaluation of OTM

Baseline impressions were obtained before orthodontic appliance placement using additional silicone impression material. Postoperative impressions were obtained at the end of the experimental period **(Figure 3A&B).** Dental casts **(Figure 3C)** were scanned using ViewBox software (version 4.1.5.5; dHAL Software, Kifissia, Greece), and digital measurements of tooth movement were performed by comparing preoperative and postoperative models **(Figure 3D).**

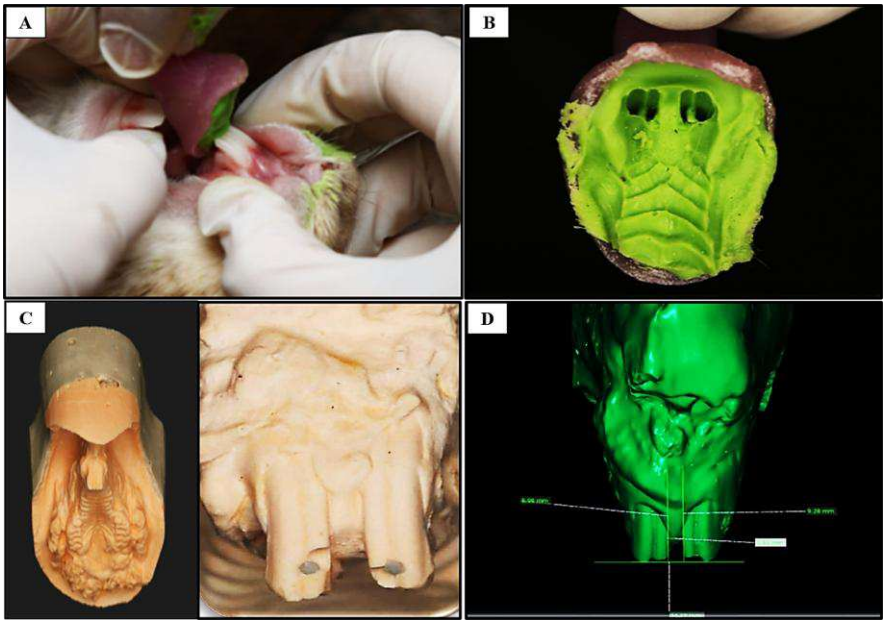


Figure 3. Measurement of OTM**. (A&B)** Steps of additional silicone impression of the maxillary incisors. **(C)** Plaster model of the maxillary incisors. **(D)** Three-dimensional illustration of the measurement performed between the two incisors.

3.11. Histological and Histomorphometric Evaluation

At the end of the experimental period, rabbits were euthanized under anesthesia using intravenous administration of an overdose of sodium pentobarbital. Following confirmation of deep anesthesia and death, intracardiac perfusion was performed according to the approved experimental protocol to facilitate tissue collection and preparation for subsequent analysis. Subsequently, maxillary specimens containing teeth and surrounding periodontal tissues were dissected and fixed in 10% neutral buffered formalin. The specimens were decalcified, processed, and embedded in paraffin blocks. Serial sections of 5 µm thickness were prepared and stained with hematoxylin and eosin (H&E) for histological examination of PDL remodeling, osteoclastic activity, and alveolar bone changes[33].

ImageJ software was used for histomorphometric analysis (National Institutes of Health, Bethesda, MD, USA) on standardized digital photomicrographs obtained from H&E-stained sections.

The following parameters were quantitatively evaluated:

- PDL width (µm): Measured as the average distance between the root surface and the adjacent alveolar bone on the pressure side.

- Osteoclast count: Determined as the number of multinucleated osteoclasts observed adjacent to the alveolar bone surface within the selected microscopic fields.
- Area percentage of remodeled bone (%): Calculated as the percentage area occupied by newly remodeled alveolar bone relative to the total examined field area.
- Vascular area percentage (%): Measured as the percentage area occupied by blood vessels within the PDL and adjacent alveolar bone
- Cellular activity score within the PDL and adjacent alveolar bone was semi-quantitatively evaluated based on the degree of fibroblastic proliferation, inflammatory cell infiltration, and osteogenic cellular activity as follows:

- Score 0 = No evident cellular activity
- Score 1 = Mild cellular activity
- Score 2 = Moderate cellular activity
- Score 3 = Marked cellular activity

A blinded examiner performed all measurements at a standardized magnification, and mean values were designed for statistical analysis. Three representative microscopic fields from each specimen were analyzed at a standardized magnification, and mean values were calculated for statistical analysis.

3.12. Statistical Analysis

Collected data from the clinical magnitude of OTM and the histomorphometry were tabularized and statistically analyzed using IBM SPSS software. Data normality was evaluated using the Shapiro–Wilk test. Data were expressed as mean ± standard deviation (SD). Quantitative assessments among the three groups were achieved utilizing Tukey's post hoc test for pairwise comparisons after one-way analysis of variance (ANOVA), the statistical significance was considered at $p \leq 0.05$.

3. Results

3.1 Characterization of the HA-NP/PRP Formulation

3.1.1. FT-IR Spectroscopy

The FT-IR spectrum of the HA-NP/PRP formulation (**Figure 4**) revealed characteristic absorption bands corresponding to the chemical functionalities of HA, along with contributions from the proteinaceous components of PRP. Firstly, the broad

band observed at 3382 cm^{-1} was mainly attributed to O–H stretching vibrations of hydroxyl groups in HA and hydrogen-bonded water, with a possible contribution from N–H stretching of PRP proteins[32]. The moderate bands detected at 2915 and 2849 cm^{-1} were associated with both symmetric and asymmetric aliphatic group C–H stretching vibrations, respectively, consistent with the HA polysaccharide backbone and possible contributions from PRP-derived biomolecules[33]. A distinct absorption band was perceived at 1734 cm^{-1}, corresponding to C=O stretching vibrations of carbonyl-containing groups. Because the spectrum represents the combined HA-NP/PRP formulation, this band may reflect contributions from both HA- and PRP-derived carbonyl-containing components; therefore, it should not be considered alone as evidence of newly formed covalent bonding. Similar carbonyl-related bands have been reported in HA- and PRP-containing biomaterials[34]. The weak band detected at 1606 cm^{-1} was primarily attributed to asymmetric stretching of the carboxylate (COO^{-}) groups in HA. However, overlap with protein-associated amide I vibrations from PRP cannot be excluded[35]. The absorption at 1217 cm^{-1} falls within the amide III/C–N vibration region and may therefore reflect contributions from PRP-derived proteins. The strong band at 1048 cm^{-1} was assigned mainly to C–O and C–O–C stretching vibrations of the HA polysaccharide backbone. The bands at approximately 970, 875, 820, and 720 cm^{-1} are located within the fingerprint region and can be assigned to skeletal and C–H vibrational modes of the HA polysaccharide structure [34]. Thus, the FT-IR spectrum retained the characteristic vibrational features of HA while showing additional protein-associated contributions from PRP, supporting the successful incorporation of both components into the final HA-NP/PRP formulation.

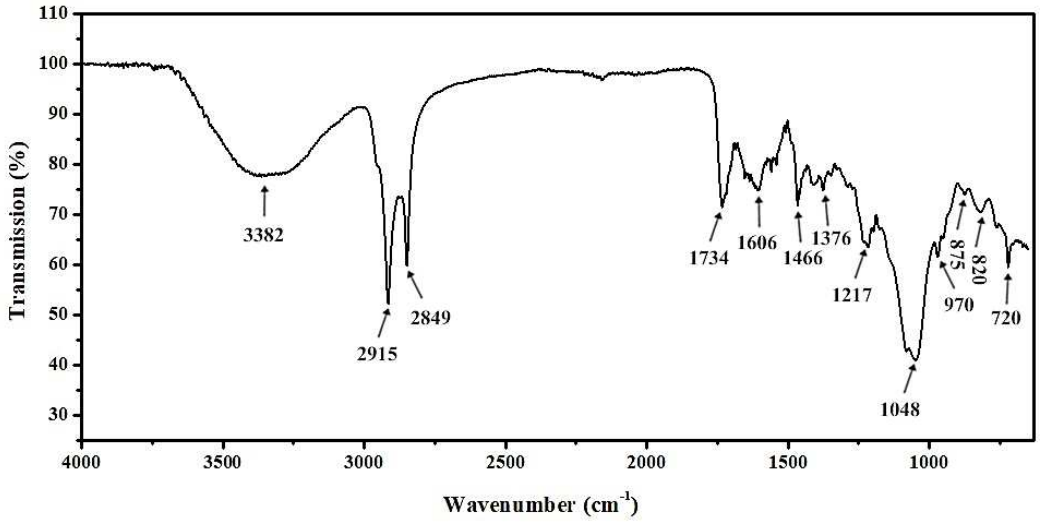


Figure 4. FTIR spectrum of the HA-NP/PRP Formulation

3.2. Morphological Analysis of the HA-NP/PRP formulation

The surface morphology of the synthezied HA-NP/PRP formulation was tested by SEM, as shown in **Figure 5A**. The micrograph reveals a heterogeneous yet interconnected architecture comprising a continuous fibrillar network decorated with numerous rounded particulate domains. The interconnected fibrillar structures are characteristic of the protein-rich matrix generated within the PRP component, which provides a three-dimensional framework that physically entraps and supports the dispersed HA nanoparticles. The presence of numerous particulate features throughout this network suggests that the HA nanoparticles were successfully incorporated into the PRP matrix rather than remaining as a completely separate phase. The relatively irregular distribution of the particles may also reflect interactions between the nanoparticles and the fibrin/protein constituents of PRP during formulation and drying. Such an integrated morphology is potentially advantageous for an injectable formulation because the fibrillar matrix can provide a structural microenvironment for nanoparticle retention while maintaining a hydrated biological interface after administration. The difference between the apparent particle dimensions observed by TEM and the larger hydrodynamic diameter determined by DLS should not necessarily be interpreted as a discrepancy. DLS measures the hydrodynamic size of particles dispersed in an aqueous medium and therefore comprises the contribution of the associated hydration layer as well as any reversible particle association. In contrast, TEM examination is performed after sample drying, during which partial dehydration

and changes in interparticle interactions can result in smaller apparent dimensions. Consequently, the two techniques provide complementary information rather than directly equivalent particle-size values. In the present HA-NP/PRP system, the TEM findings therefore support the formation of nanoscale HA domains. On the other hand, the DLS results provide information regarding their effective size and dispersion behavior in the hydrated state. Thus, the SEM and HR-TEM findings demonstrate that the HA nanoparticles are incorporated within a fibrillar PRP-derived matrix while retaining a distinct nanoscale morphology. The combination of a three-dimensional protein/fibrin framework and nano-sized HA domains may present a favorable structural basis for the intended biological application, potentially facilitating nanoparticle retention and interaction with the surrounding biological environment.

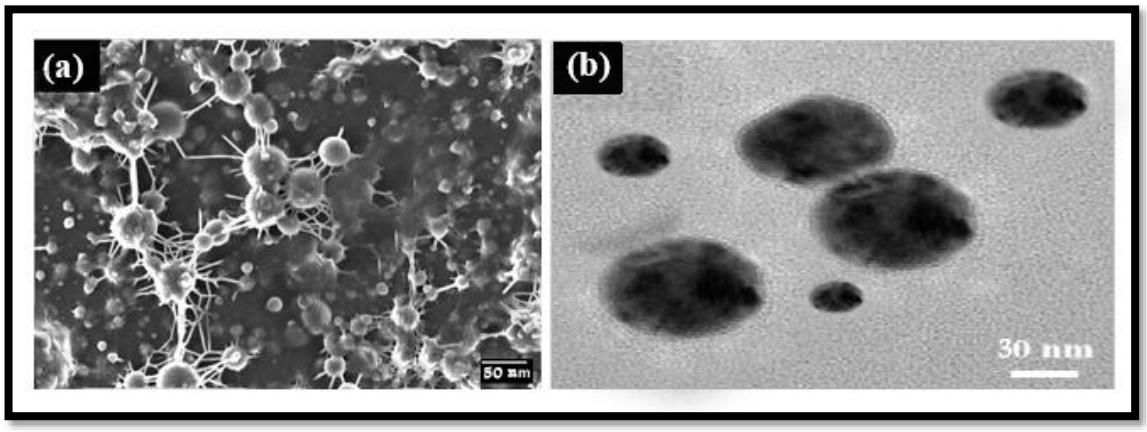


Figure 5. (A) SEM-image of HA-NP/PRP Formulation. **(B)** HR-TEM image of HA-NP/PRP Formulation

3.3. Particle Size, Polydispersity Index, and Zeta Potential

polydispersity index (PDI), particle size, and zeta potential of the prepared HA nanoparticles were measured before PRP incorporation. These measurements were carried out on the HA nanoparticle dispersion before preparation of the final HA-NP/PRP formulation, which was prepared immediately before administration and was not intended for long-term storage. The nanoparticle dispersion was appropriately diluted with deionized water before analysis. Samples intended for particle-size and PDI measurements were transferred into square glass cuvettes, whereas zeta-potential

measurements were performed using transparent disposable zeta cells. All measurements were performed in triplicate under identical experimental conditions. The prepared HA nanoparticles revealed a mean hydrodynamic particle size of 153.2 ± 4.8 nm and a PDI of 0.35 ± 0.03, indicating a moderately broad particle-size distribution. A negative zeta potential of −27.4 ± 1.5 mV was observed, which may be linked to the ionized carboxylate groups of HA and suggests moderate electrostatic stabilization of the nanoparticle dispersion. The corresponding particle size, PDI, and zeta potential values are summarized in **Table 1.**

Table 1. Particle size, polydispersity index, and zeta potential of the prepared HA nanoparticles

Formulation	Particle size (nm)	PDI	Zeta potential (mV)
HA nanoparticles	153.2 ± 4.8	0.35 ± 0.03	−27.4 ± 1.5

3.4. Viscosity and Rheological Behavior

The HA-NP/PRP formulation possessed a viscosity of 1050 ± 30 cP at 20 rpm and 25 ± 0.5 °C. This value indicates a moderately viscous formulation with sufficient internal resistance to flow while maintaining a relatively fluid consistency. The obtained viscosity can be associated with the combined contributions of the HA polymeric phase and the protein-rich PRP matrix, with intermolecular interactions between these components increasing the overall resistance to flow[22]. The incorporation of HA nanoparticles may further modify the flow behavior by increasing the effective dispersed-phase content within the formulation. The relatively uniform viscosity observed across the measurements, as reflected by the small standard deviation, indicates good consistency of the prepared formulation under the tested conditions. From a formulation perspective, the measured viscosity represents a balance between structural cohesion and flowability, which is desirable for a locally administered injectable system. However, because viscosity is dependent on shear rate, temperature, and measurement conditions, the present value should be interpreted specifically under the applied experimental conditions rather than as an intrinsic constant of the formulation. Generally, the measured viscosity supports the physicochemical suitability of the HA-NP/PRP formulation for further evaluation as an injectable preparation.

3.1. Clinical Evaluation of OTM

All experimental groups demonstrated OTM following force application. Both the LLLT group and the HA-NP/PRP group showed slightly greater mean OTM (1.29 ± 0.10 and 1.37 ± 0.12, respectively) than the control group (1.12 ± 0.08). Although the HA-NP/PRP group exhibited the greatest mean OTM, followed by the LLLT group, the overall difference among the three groups was not statistically significant (p = 0.084). **(Table 2 and Figure 6).**

Table 2. Quantitative Measurement of OTM Among the Studied Groups

Group	n	OTM (mm), Mean ± SD
Control		1.12 ± 0.08[a]
LLLT		1.29 ± 0.10[a]
HA-NP/PRP		1.37 ± 0.12[a]
Overall p-value		**0.084**

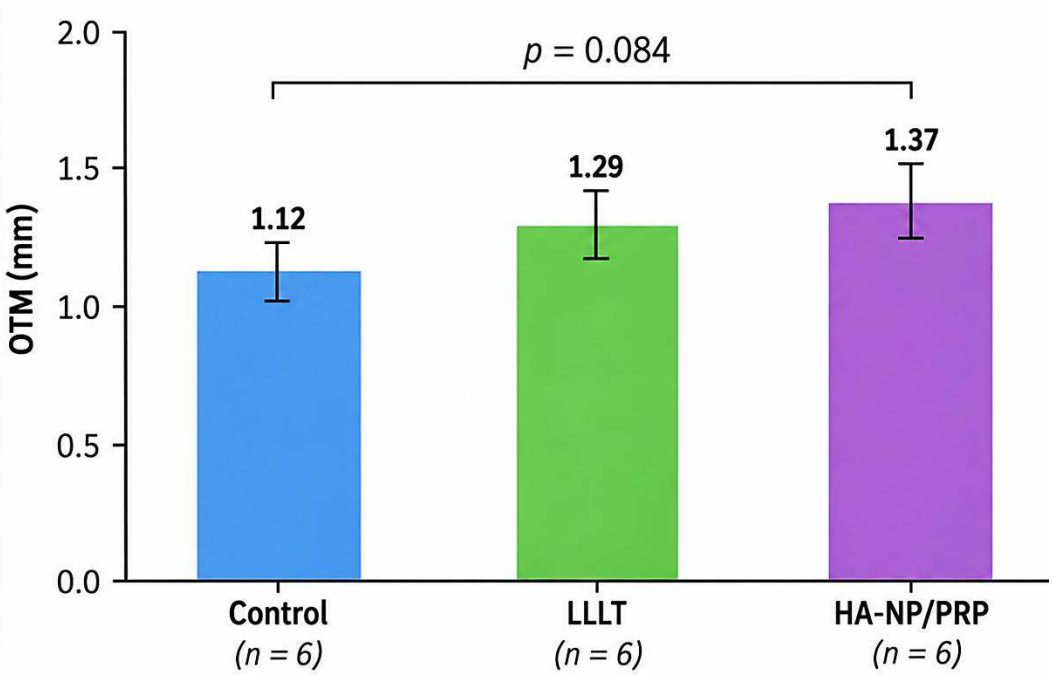


Figure 6: Quantitative measurement of orthodontic tooth movement in the studied groups. Data are mean ± SD. The highest mean orthodontic tooth movement was seen in the HA + PRP group, followed by the Laser and Control groups. However, the overall group difference was not statistically significant (p = 0.084).

3.2. Histological Findings

3.2.1. Interdental septum:

Group I (+Ve Control) showed the least thickness of the interdental septum and bone trabeculae among all groups. In contrast, the HA-NP/PRP group showed the greatest thickness, exceeding that of group II (LLLT). All groups demonstrated large osteocytes, which appeared irregularly distributed in the control and were uniformly distributed in both group II and III. All groups showed clearly visible, deeply stained resting lines, which appeared thin and scarce in the control and were present in several in both group II and III **(Figure 7 D1-D3).**

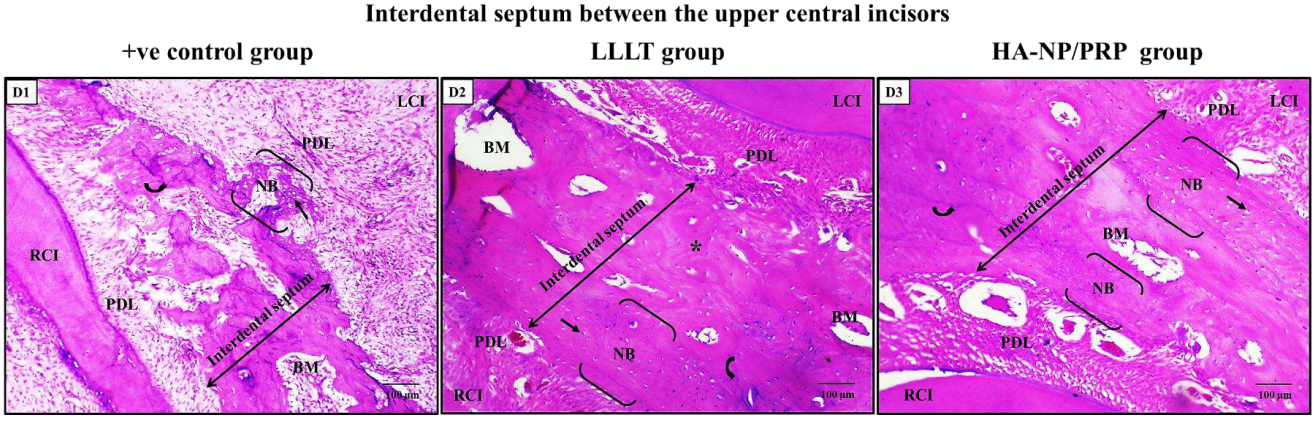


Figure 7. Photomicrographs of the interdental for all groups. **D1 (+Ve Control Group):** displaying broad, irregular bone marrow gaps (BM), a thin interdental septum with thin bone trabeculae, and uneven bone matrix architecture, and thin, deeply stained resting bone lines (curved arrow). Numerous irregularly distributed osteocytes (straight arrow). The PDL areas adjacent to the left and right central incisors (LCI, RCI) exhibit unevenly aligned fibers and appear disordered. Notice the small thickness of the interdental septum (double-ended arrow) and the small amount of newly formed bone (NB) in between the brackets (). **D2 (LLLT Group):** displaying a more ordered lamellar bone with several resting lines (curved arrows), a moderately substantial interdental septum, and bone trabeculae surrounding broad, irregular bone marrow voids (BM). It is possible to show several uniformly distributed osteocytes (straight arrow). Fiber bundles with a more uniform, oblique orientation toward the root surfaces are visible in the PDLs of both RCI and LCI. Notice the larger thickness of the interdental septum (double-ended arrow), and the moderate amount of newly formed bone (NB) inside the brackets (). **D3 (HA-NP/PRP Group):** demonstrating a thicker interdental septum (double-ended arrow), with more vascularized BM gaps and well-organized bone trabeculae. Additionally shown are numerous large osteocytes (straight arrow) and several clearly visible resting lines (curved arrow). From the roots of RCI and LCI to the alveolar bone, the PDL fibers show respectable organization. Notice the moderate amount of newly formed bone (NB) inside the brackets (). (H&E stain X100).

3.2.2. Compression side/distal root side of the right and left central incisors (RCI and LCI).

+ve Control Group: The compressive force significantly disrupts the PDL architecture. It appeared thin with disorganized collagen fibers, and the alveolar bone exhibited broad BM gaps filled with extravasated blood and thin, irregular trabeculae. Disorganized bone deposition appeared as sparse, disturbed resting lines, several large osteocytes, and multiple resorptive areas on the bone surface (Figure 8C1**).**

LLLT Group: The PDL showed a moderate level of structural preservation. Its fiber bundles were inserted into the root surface at a higher density and alignment, with numerous active cementoblasts on the surface. Large irregular bone marrow spaces surrounded by thick trabeculae of bone and contained numerous large osteocytes with numerous resorptive regions that were limited to a tiny portion of the bone's surface **(Figure 8 C2).**

HA-NP/PRP Group: PDL appeared as densely packed, well-oriented collagen fibers containing several active fibroblasts and inserted into the root surface, which was lined with active cementoblasts. The alveolar bone had a clearly defined incremental resting line separating the newly created bone from the native old bone. Large irregular marrow spaces with extravasated blood and numerous large osteocytes were detected in both **(Figure 8 C3).**

As a result of compressive force, areas of active bone resorption in all groups showed osteocytes densely packed within the lacunae of the bone matrix. Also, the Howship's lacunae of bone-resorbing regions contain enormous, multinucleated giant cells, numerous large active fibroblasts, and less organized collagen fiber bundles that integrate into the remodeling bone front in the highly vascularized PDL region **(Figure 8 C4).**

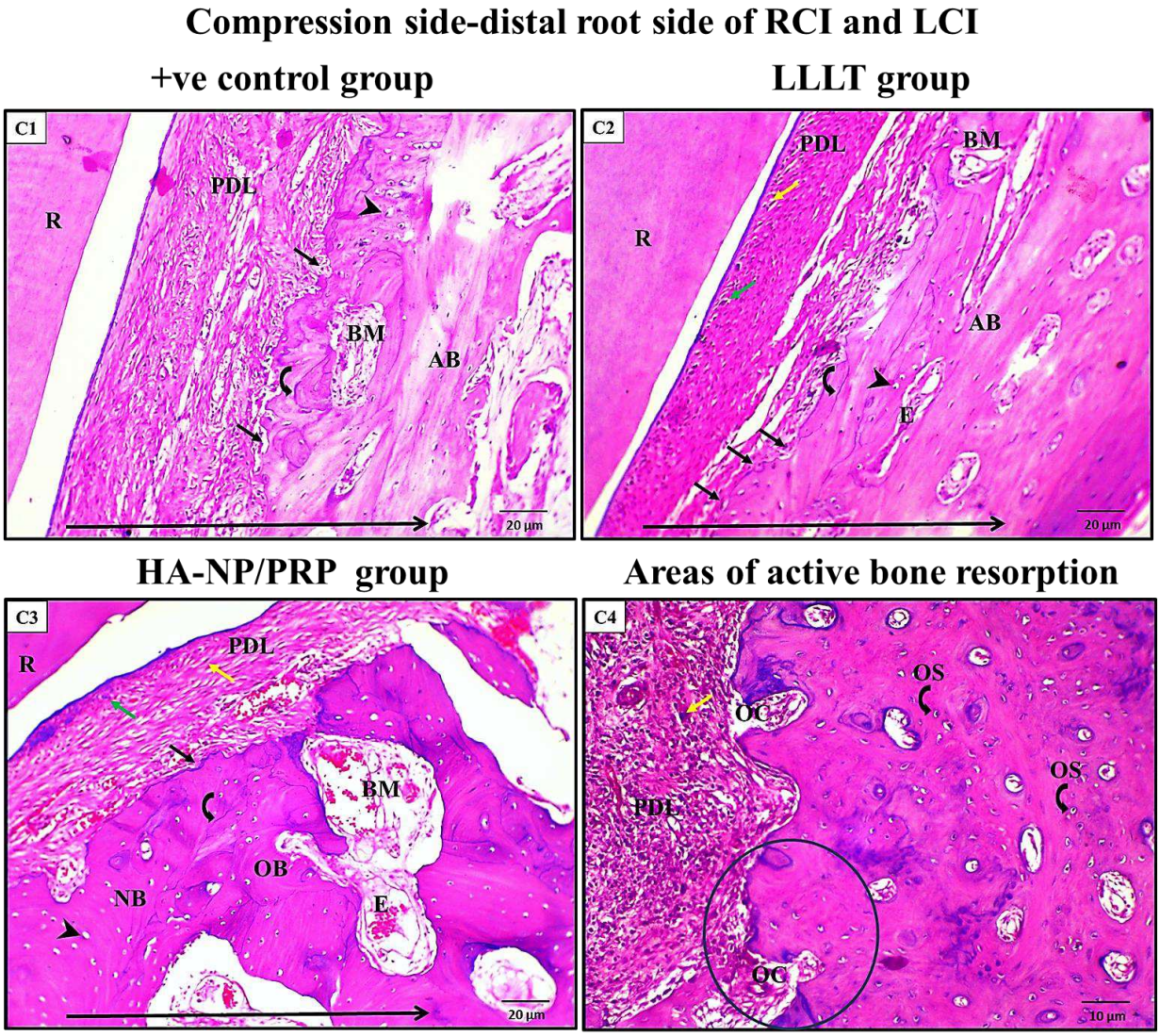


Figure 8. Photomicrographs of each group's distal and compression side. **C1 (+ve Control Group):** The compressive force significantly disrupts the PDL architecture. In the direction of the root surface (R), it appears thin with disorganized collagen fibers. The alveolar bone (AB) exhibits broad BM gaps filled with extravasated blood (E) and thin, irregular trabeculae. Disorganized bone deposition is suggested by sparse and disturbed resting lines (curved arrow). Several large osteocytes are also seen (arrowhead). Notice the multiple resorptive areas on the bone surface (straight arrows). **C2 (LLLT Group):** The PDL shows a moderate level of structural preservation. Its fiber bundles insert into the root surface (R) with better density and alignment. Notice the numerous active cementoblasts on the root surface (green arrows). Large irregular BM gaps with extravasated blood (E) are seen in AB. These spaces are surrounded by thick trabeculae of bone that contain numerous large osteocytes (arrowhead). Notice the numerous resorptive regions that are limited to a tiny portion of the bone's surface (straight arrows).

C3 (HA-NP/PRP Group): PDL is shown as densely packed, well-oriented collagen fibers, which are lined with active cementoblasts (green arrows) that insert into the root surface (R) and contain several active fibroblasts (yellow arrows). The AB displays a clearly defined incremental resting line (curved arrow) separating the newly created bone (NB) from the native old bone (OB). Large irregular BM spaces with extravasated blood (E), and numerous large osteocytes (curved arrows) are visible in both forms of bone. **C4 (A high magnification of areas of active bone resorption):** Osteocytes appear to be densely packed within the lacunae of the bone matrix (OS, curved arrows). Additionally, the Howship's lacunae of bone-resorbing regions contain massive, multinucleated, giant cells (osteoclasts, OC) (circled area). Also, the numerous big active fibroblast cells (yellow arrows) and less organized collagen fiber bundles that integrate into the remodeling bone front in the highly vascularized PDL region. The orthodontic force direction is indicated by the arrow in the lower portion of each photomicrograph. (H&E stain C1, C2, and C3 X 400; C4 X1000).

3.2.3. Tension side/mesial root side of the right and left central incisors (RCI and LCI).

+ve Control Group: A disturbed PDL resulting from the applied tension force was observed, with dense fibers containing active fibroblasts inserted into the root surface. The alveolar bone was composed mostly of immature woven bone, with broad, irregular marrow spaces containing extravasated blood and numerous, irregularly distributed osteocytes **(Figure 9 T1).**

LLLT Group: The PDL appeared more ordered, with numerous fibroblasts and dense bundles of collagen fibers, and a highly active cementoblast layer lining the root surface. The alveolar bone showed a heavily stained line separating immature new bone from old native bone. Additionally, a considerable number of recently entrapped

osteocytes and well-formed marrow spaces with highly vascularized areas were depicted **(Figure 9 T2).**

HA-NP/PRP Group: Improved density and organization were seen in the PDL fiber bundles, which contained active fibroblasts and extended toward the root surface, which was surrounded by an orderly alignment of active cementoblasts. Large regions of newly formed bone, with numerous, unevenly distributed osteocytes and a deeply stained line separating it from the old native bone, were seen in the alveolar bone, with discrete marrow spaces. Additionally, there was active osteoblastic bone deposition on the surface. **(Figure 9 T3).**

As a result of tension force**,** areas of active bone deposition are created. The woven bone was observed interacting with the newly formed bone matrix. The interface between the new bone and the native old bone of the socket wall is also marked by a deeply stained line. Active fibroblasts were seen within the PDL fibers and surrounding vascularized interstitial tissues; plump, active osteocytes were frequently embedded within their lacunae throughout the matrix; and active osteoblasts were seen lining the bone surface **(Figure 9 T4).**

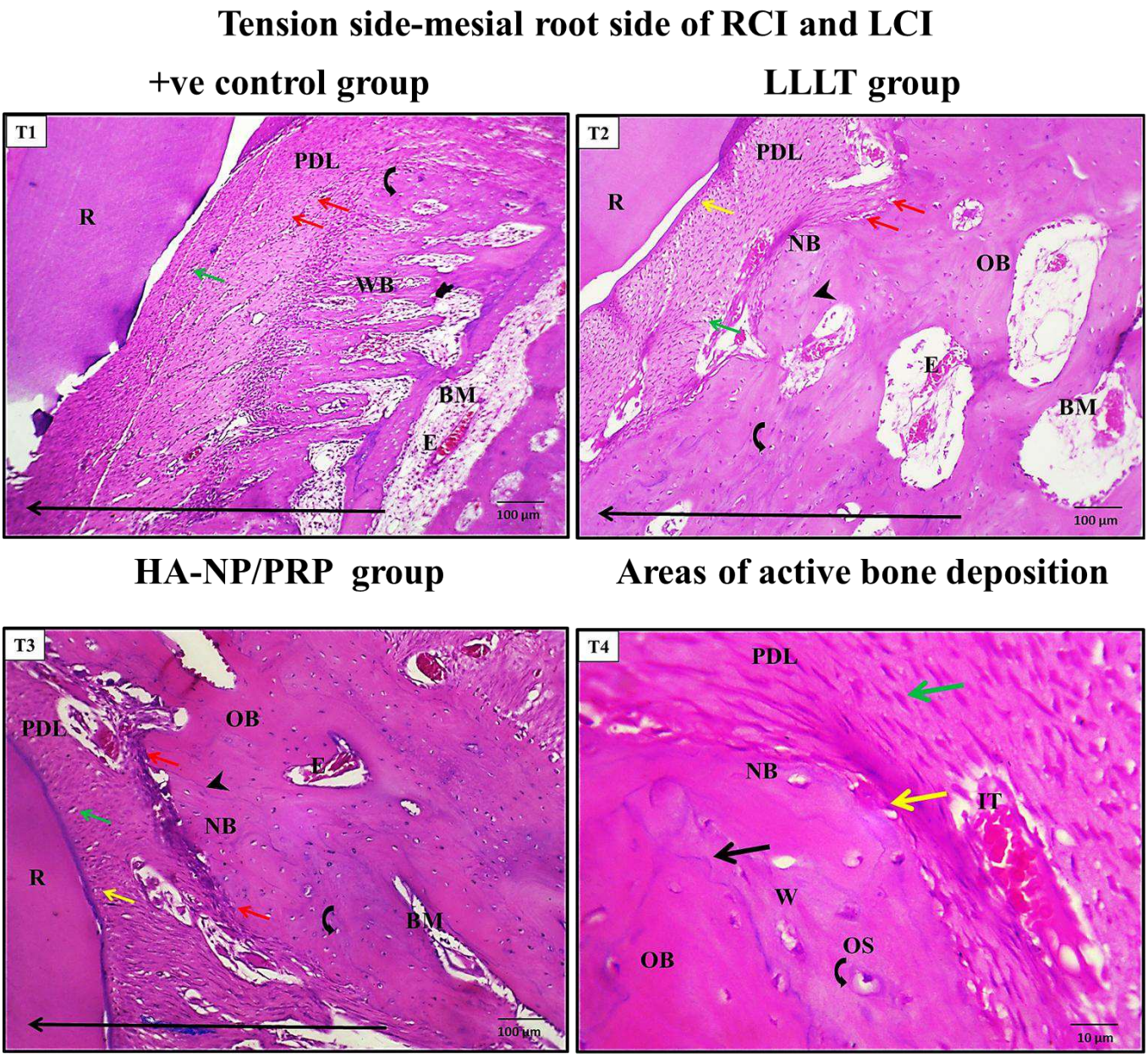


Figure 9. Photomicrographs of the **tension/mesial side** of all groups. **T1 (+ve Control Group):** displaying disturbed PDL as a result of the tension force applied; its dense fibers insert into the root surface (R) with active fibroblasts (green arrow). The AB is mostly made up of immature woven bone (WB) with broad, irregular BM spaces with extravasated blood (E) and large, many, irregularly distributed osteocytes (curved arrow). **T2 (LLLT Group):** The PDL, which has many fibroblasts and dense bundles of collagen fibers, appears more ordered (green arrow). A highly active cementoblast layer (yellow arrow) that lines the root surface (R) is where the fibers are immediately attached. The AB shows a heavily stained line (arrowhead) separating immature new bone (NB) from old native bone (OB). Additionally, a considerable number of recently entrapped osteocytes (curved arrows) and well-formed BM gaps with highly vascularized areas (E) are depicted. **T3 (HA-NP/PRP Group):** Improved density and organization are seen in the PDL fiber bundles, which contain active fibroblasts (green arrow) and extend toward the root surface (R), which is surrounded by an orderly alignment of active cementoblasts (yellow arrows). Large regions of newly formed bone (NB) with numerous, unevenly distributed osteocytes (curved arrow) and a deeply stained line

(arrow head) separating it from the old native bone (OB) can be seen in the AB. Additionally, discrete BM spaces and extravasated blood (E) may be shown. Additionally, there is active osteoblastic surface bone deposition (red arrows). **T4 (A high magnification of areas of active bone deposition):** The vestiges of original woven bone (W), shown by clear, deeply stained resting lines (black arrow), are seen interacting with the freshly produced bone matrix (NB). The interface between the NB and the native old bone (OB) of the socket wall is also marked by a similar line. Active fibroblasts are seen within the PDL fibers and surrounding vascularized interstitial tissues (IT); active, plump osteocytes (OS, curved arrows) are frequently embedded within their lacunae throughout the matrix; and active osteoblasts (yellow arrow) are seen lining the bone surface. The orthodontic force direction is indicated by the arrow in the lower portion of each photomicrograph. (H&E stain T1, T2, and T3 X 400; T4 X1000).

3.3. Histomorphometric Results:

Detailed quantitative histomorphometric measurements are presented in **Table 3 and Figure 10.** Also, the raw histomorphometric measurements obtained from all experimental groups are presented in Supplementary Tables 1-5.

Table 3. Histomorphometric Measurements Among the Studied Group. Values are expressed as mean ± standard deviation (SD). n = 6 per group.

Parameter	+ve control group	LLLT Group	HA-NP/PRP Group	p-value
PDL width (µm)	112.4 ± 8.3^{a}	138.7 ± 10.2^{b}	156.9 ± 12.1^{c}	0.021*
Osteoclast count	4.2 ± 1.1^{a}	6.8 ± 1.4^{b}	8.9 ± 1.7^{c}	0.015*
Remodeled bone area (%)	18.6 ± 3.4^{a}	27.3 ± 4.1^{b}	35.8 ± 5.2^{c}	0.008*
Vascular area percentage (%)	11.17 ± 1.47^{a}	16.67 ± 1.86	22.50 ± 2.17	0.001*
Cellular activity score	0.75 ± 1.83^{a}	0.75 ± 2.83^{b}	1.17 ± 4.17^{c}	0.006*

*Statistically significant at $p \leq 0.05$. Different superscript letters indicate statistically significant differences between groups.

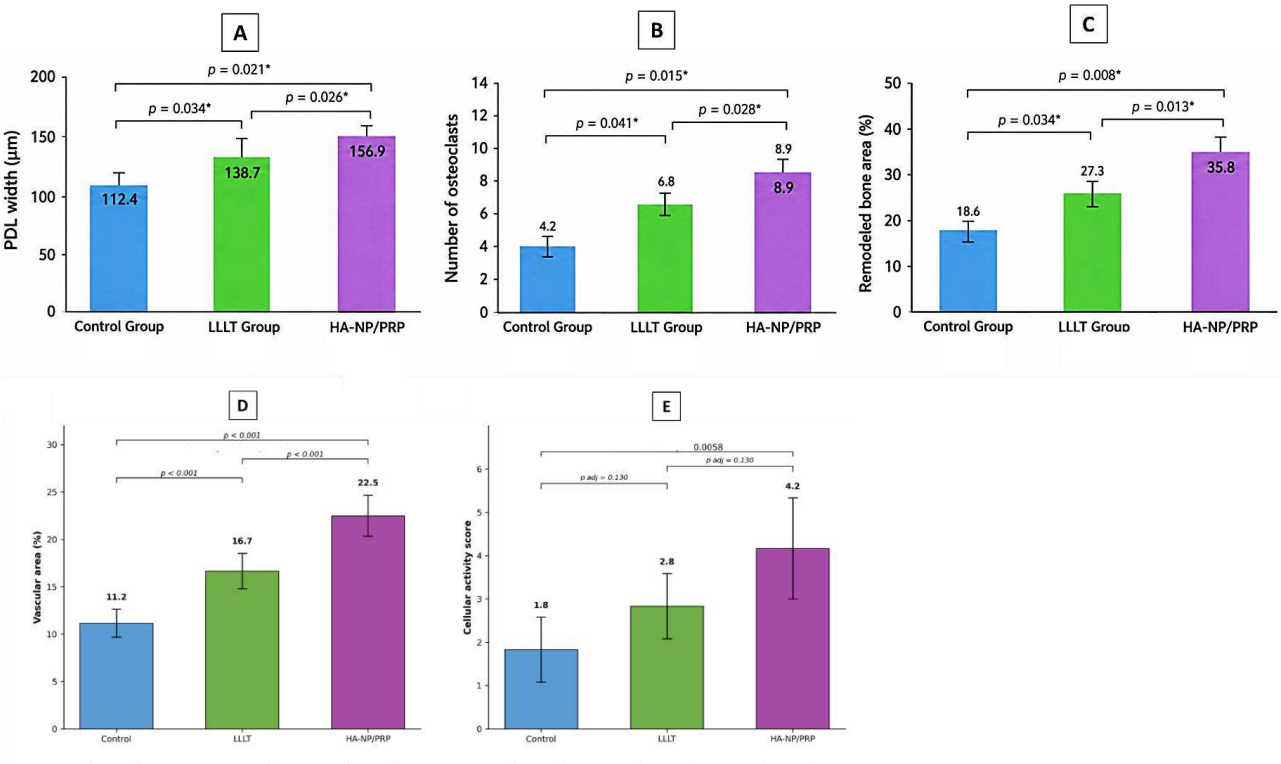


Figure 10. Histomorphometric analysis of PDL and alveolar bone remodeling characteristics between the experimental groups (control, LLLT, HA-NP/PRP). n = 6 per group, the data are presented as mean ± standard deviation (SD). ANOVA and Tukey's post hoc test were used for statistical comparisons. Statistically significant differences ($p < 0.05$) are indicated by asterisks.

The PDL width values in both the LLLT and HA-NP/PRP groups were significantly higher than those in the control group ($p < 0.001$ for both groups). Moreover, the largest mean PDL width was observed in the HA-NP/PRP group, and a significant difference ($p < 0.001$) was found between the LLLT and HA-NP/PRP groups. The number of osteoclasts was significantly increased in the LLLT group ($p=0.0165$) and HA-NP/PRP group ($p<0.001$) when compared with the control group. However, there was no statistically significant difference between the LLLT and HA-NP/PRP groups ($p = 0.0537$). Bone regeneration was significantly greater in the LLLT and HA-NP/PRP groups compared to the control group ($p = 0.0084$ and $p < 0.001$, respectively). The difference between LLLT and HA-NP/PRP was significant ($p = 0.0099$), and the largest mean rebuilt bone area was in the HA-NP/PRP group. The vascular area % values were significantly higher in the LLLT and HA-NP/PRP groups than in the control group ($p = 0.0014$ and $p < 0.001$, respectively). Also, the vascular area (%) in the HA-NP/PRP group was significantly higher than in the LLLT group ($p = 0.0206$). There was no significant difference in cellular activity score between the LLLT group and the control group or the HA-NP/PRP group ($p=0.130$ for both comparisons). However, the difference in cellular activity score between the control and HA-NP/PRP groups was statistically significant ($p=0.013$), with the HA-NP/PRP group showing a higher score.

4. Discussion

Notably, the long duration of orthodontic treatment is one of the major challenges in clinical orthodontics due to its association with patient discomfort, increased risk of enamel demineralization, gingival inflammation, root resorption, and poor patient compliance[36, 37]. Research has therefore focused on developing minimally invasive procedures to expedite OTM while maintaining the integrity of periodontal tissue [38]. The present study comparatively evaluated the effects of LLLT and an injectable HA formulation mixed with PRP on OTM in rabbits, using clinical, histological, and histomorphometric assessments.

In our present study, both experimental groups showed slightly more OTM than the control group. However, the quantitative differences between groups were statistically non-significant ($p > 0.05$). Although tooth movement measurements showed limited differences, histological and histomorphometric results revealed

increased periodontal remodeling and alveolar bone activity in the experimental groups, especially in the HA-NP/PRP group.

The effects observed with LLLT may be due to its photobiomodulation effect on periodontal and bone cells. Previous studies have shown that low-level laser irradiation promotes cellular metabolism, increases ATP production, stimulates angiogenesis, and enhances osteoclastic and osteoblastic activity, thereby accelerating bone remodeling during OTM [39, 40]. In the present study, vascularity and moderate osteoclastic activity were noted in the LLLT group. PDL spaces increased compared with the control group, consistent with previous reports describing the stimulatory effect of diode lasers on periodontal tissue remodeling[39, 41].

Interestingly, the combination of an injectable hyaluronic acid formulation with PRP showed better histological and histomorphometric characteristics than the control or LLLT groups. This finding may be attributed to the biological effect of both HA and PRP in tissue regeneration. In addition, HA was confirmed to increase PDL cellular proliferation and attachment, modulate inflammatory responses, and promote osteogenic activity [42, 43]. However, PRP provides growth factors that encourage cell recruitment, proliferation, and tissue restoration[22]. In addition, PRP contains several growth factors, such as vascular endothelial growth factor (VEGF), transforming growth factor beta (TGF-β), and platelet-derived growth factor (PDGF), which are vital for angiogenesis, cellular proliferation, and bone remodeling[44, 45]. These growth factors may enhance osteoclastic recruitment and accelerate periodontal tissue turnover during OTM[46].

HA also has anti-inflammatory and wound-healing properties and may promote periodontal tissue regeneration [42, 47]. HA may maintain a hydrated microenvironment within periodontal tissues and promote cellular migration, proliferation, and extracellular matrix remodeling through its interactions with extracellular matrix components and cell-surface receptors. Furthermore, HA-based injectable formulations can be used as local delivery matrices for bioactive molecules. However, the formulation employed in the present study needs to be experimentally confirmed to determine whether it improves the retention or sustained release of PRP-derived growth factors[42].

The histological findings of increased cellularity and improved vascularization in Group III (HA-NP/PRP) could indicate more active remodeling of the alveolar bone and PDL. Furthermore, the more organized PDL fibers in this group may indicate better tissue adaptation during the application of orthodontic force[42, 45]. The current study's findings are in line with earlier research demonstrating that PRP application may affect alveolar bone remodeling and OTM [46, 48]. Similarly, experimental studies have shown that low-level laser therapy can modulate periodontal vascularization and osteoclastic activity during OTM [49]. Such effects could be explained by the capacity of PRP-derived growth factors and laser-mediated photobiomodulation to influence cellular responses involved in periodontal tissue remodeling; however, the magnitude and direction of these effects are protocol-dependent.

The relatively small quantitative differences in OTM, compared with the more marked histological changes, may be partly explained by the short duration of the experiments and the dynamic nature of periodontal tissue remodeling. Following the application of orthodontic force, cellular and vascular responses occur within the PDL, initiating a cascade of biological events that control alveolar bone resorption and formation. These early tissue responses may not necessarily translate into measurable differences in tooth movement, as tooth displacement occurs through coordinated, time-dependent remodeling processes. This interpretation is consistent with experimental studies demonstrating temporal changes in alveolar bone morphology during OTM and with reviews highlighting the complex relationship between biological responses and tooth displacement [50, 51].

The rabbit model in our study was a useful experimental system for evaluating histological responses in alveolar bone and periodontal tissues following the solicitation of orthodontic forces. However, species differences in dental anatomy and bone remodeling should be considered when extrapolating these findings to humans. In addition, minimally invasive injectable biologic approaches, such as PRP-based therapies, may offer an alternative to surgically assisted orthodontic acceleration techniques. But their clinical effectiveness and safety require further investigation in well-designed human studies [46, 52].

Conclusion

Considering the outcomes of the present study, both LLLT and HA-NP/PRP possess potential to improve OTM and stimulate periodontal tissue regeneration. No statistically significant quantitative differences in tooth movement were observed among groups, but HA-NP/PRP showed more favorable histological and histomorphometric results for PDL remodeling, vascularity, and alveolar bone activity. HA-NP/PRP is a promising, minimally invasive adjunctive approach to enhancing biologic responses during orthodontic treatment.

Limitations

1- The observation time was short, and the number of samples was small, so this could be a reason for the magnitude of measurable clinical tooth movement.
2- The study was mainly based on histological and histomorphometric assessments and did not assess immunohistochemical or molecular biomarkers of bone remodeling and inflammatory responses.

Thus, Future studies with molecular analyses and longer follow-up periods could offer more understanding of the biological processes underlying orthodontic acceleration by bioactive injectable formulations.

Declarations

Ethics Approval and Consent to Participate: All experimental procedures performed in this study were approved by the Research Ethics Committee, Faculty of Dentistry, Pharos University in Alexandria, Egypt, and were conducted in accordance with institutional guidelines for the care and use of laboratory animals and ARRIVE 2.0 guidelines.

Consent for Publication: Not applicable.

Availability of Data and Materials: The datasets generated and analyzed during the current study are available from the corresponding author upon reasonable request.

Competing Interests: The authors declare that they have no competing interests.

Funding: The authors received no financial support for the research, authorship, or publication of this article.

Authors' Contributions: Hani AlSwafeeri contributed to the study conception and design, orthodontic procedures, supervision of orthodontic force application, and manuscript revision. **Wafaa Yahia Alghonemy** contributed to the histological evaluation and interpretation of histopathological findings, as well as to writing and revision of the manuscript. **Rehab El Sharkawy** contributed to the preparation and characterization of the injectable hyaluronic acid formulation and participated in data interpretation and manuscript revision. **Rania A. Hanafy** contributed to biomaterial preparation, material characterization, and the interpretation of the results obtained. **Menna Galal Beshara** contributed to animal handling, orthodontic procedures, data collection, and clinical measurements. **Khaled AboulAzm** contributed to the placement of orthodontic appliances, experimental procedures, and data acquisition. **Eman M. Salem** contributed to study design, histological and histomorphometric analysis, data interpretation, manuscript writing, and final revision of the manuscript. All authors read and approved the final manuscript.

Abbreviations

LLLT: Low-level laser therapy
PRP: Platelet-rich plasma
HA: Hyaluronic acid
OTM: Orthodontic tooth movement
PDL: Periodontal ligament
H&E: Hematoxylin and eosin

SEM: Scanning electron microscopy
FTIR: Fourier transform infrared spectroscopy

References:

1. Zhao Z, Chen L, Zhu S, Yu H, Chen Y, Song J, et al. Periodontal ligament stem cells in tissue remodeling: from mechanical forces to inflammatory signals. Stem Cell Res Ther. 2025;16:653.

2. Hamidaddin MA. Optimal treatment timing in orthodontics: A scoping review. Eur J Dent. 2024;18:86–96.

3. Elshenawy EA, Alawy SB, Alghonemy WY, El Dosoky AI. Preventing white spot lesions around orthodontic brackets: efficacy of pre-reacted glass-ionomer barrier coat versus silver diamine fluoride: an in vitro study. BDJ open. 2025;11:45.

4. Gao Y, Min Q, Li X, Liu L, Lv Y, Xu W, et al. Immune system acts on orthodontic tooth movement: cellular and molecular mechanisms. Biomed Res Int. 2022;2022:9668610.

5. Zheng Y, Lam XY, Wu M, Lin Y. Acceleration of orthodontic tooth movement: A bibliometric and visual analysis. Int Dent J. 2025;75:1223–33.

6. Keser E, Naini FB. Accelerated orthodontic tooth movement: surgical techniques and the regional acceleratory phenomenon. Maxillofac Plast Reconstr Surg. 2022; 44 (1). Chinese J Tissue Eng Res www CJTER com.

7. Tsolakis IA, Christopoulou I, Sitaras S, Lyros I, Rontogianni A, Dalampira M, et al. Molecular and biological aspects of orthodontic tooth movement: possibilities for bioengineering intervention: a narrative review. Bioengineering. 2023;10:1275.

8. Elgadi R, Sedky Y, Franzen R. The effectiveness of low-level laser therapy on orthodontic tooth movement: a systematic review. Lasers Dent Sci. 2023;7:129–37.

9. Garzón J, Baldion PA, Grajales M, Escobar LM. Response of osteoblastic cells to low-level laser treatment: a systematic review. Lasers Med Sci. 2022;37:3031–49.

10. Rando RG, Buchaim DV, Cola PC, Buchaim RL. Effects of photobiomodulation using low-level laser therapy on alveolar bone repair. In: Photonics. MDPI; 2023. p. 734.

11. Alam MK, Hajeer MY, Alanazi DA, Alanazi SA, Alruwaili HO. The effect of low-level laser therapy on accelerating tooth movement in orthodontic patients: A randomized controlled trial. J Pharm Bioallied Sci. 2024;16 Suppl 4:S3658–60.

12. Özsoy B, Güldüren K, Kamiloğlu B. Effect of low-level laser therapy on orthodontic tooth movement during miniscrew-supported maxillary molar distalization in humans: a single-blind, randomized controlled clinical trial. Lasers Med Sci. 2023;38:76.

13. Farhadian N, Miresmaeili A, Borjali M, Salehisaheb H, Farhadian M, Rezaei-Soufi

L, et al. The effect of intra-oral LED device and low-level laser therapy on orthodontic tooth movement in young adults: a randomized controlled trial. Int Orthod 19 (4): 612–621. 2021.

14. Yassaei S, Fekrazad R, Shahraki N. Effect of low level laser therapy on orthodontic tooth movement: a review article. J Dent (Tehran). 2013;10:264.

15. Elnaggar YSR, Zewail M, Salem EM, Alghonemy WY, Ahmed NM, Abdelfatah OM, et al. Development and Appraisal of Luteolin-Loaded Nanohyaluosomes as a Sustainable Tissue Engineering Nanotherapy for Treatment of Periodontitis: Biochemical and Biological Investigations. J Drug Deliv Sci Technol. 2026;:107957.

16. Hanafy RA, El-Sharkawy RM, Salem EM, Ahmed NM, Abdelfatah OM, Alghonemy WY. Development of a chitosan-hydroxypropyl methylcellulose/nano-fluorapatite hydrogel as a novel biomaterial for enhanced post-tooth extraction bone healing in diabetic conditions. RSC Adv. 2026;16:7230–51.

17. Atia GA, Ali MA, Abdeen A, Alghonemy WY, Zakarya A, Shaban EE, et al. Recombinant Biologics in periodontal and peri-implant reconstruction: Advances, delivery strategies, and translational challenges. J Drug Deliv Sci Technol. 2026;:108140.

18. Sheykhhasan M, Seifalian A. Plasma-rich in growth factor and its clinical application. Curr Stem Cell Res Ther. 2021;16:730–44.

19. Elghonamy WYI, Gaballah OM, El Amy SA. Effect of platelet rich plasma on regeneration of submandibular salivary gland of albino rats. system. 2018;1.

20. Anitua E, Allende M, Alkhraisat MH. Unravelling alveolar bone regeneration ability of platelet-rich plasma: a systematic review with meta-analysis. Bioengineering. 2022;9:506.

21. Gonçalves A, Barros G, Coelho M, Monteiro F, Silva FS, Pinho T. Effectiveness of surgical and non-surgical techniques for accelerating orthodontic tooth movement in fixed appliances and aligners: a systematic review. Turkish J Orthod. 2025;38:64.

22. Alghonemy WY, Ahmed NM, Abou Samra AA, Abdelfatah OM, Hanafy RA, Abd El-Aziz AM, et al. Enhanced periodontal regeneration using formulated injectable hyaluronic acid with or without PRP: A rat ligature model. J Oral Biol Craniofacial Res. 2026;16:101465.

23. Mourad D, Goymen M, Uzuner FD, Onal T, Tuglu MI. Injectable hyaluronic acid: a method for accelerating alveolar bone remodelling during orthodontic tooth movement. Australas Orthod J. 2025;40:172–83.

24. Chęciński M, Lubecka K, Bliźniak F, Chlubek D, Sikora M. Hyaluronic acid/platelet-rich plasma mixture improves temporomandibular joint biomechanics: A systematic review. Int J Mol Sci. 2024;25:9401.

25. Percie du Sert N, Hurst V, Ahluwalia A, Alam S, Avey MT, Baker M, et al. The ARRIVE guidelines 2.0: Updated guidelines for reporting animal research. J Cereb Blood Flow Metab. 2020;40:1769–77.

26. Alawy SB, El Meligy MAA, Salem EM, Alghonemy WY. Impact of concentrated

growth factor (CGF) injection on acceleration of orthodontic tooth movement in rabbits. BMC Oral Health. 2024;24:783.

27. Faul F, Erdfelder E, Lang A-G, Buchner A. G* Power 3: A flexible statistical power analysis program for the social, behavioral, and biomedical sciences. Behav Res Methods. 2007;39:175–91.

28. Pippin JJ, Bailey J, Kennedy M, Press DD, McCarthy J, Baron R, et al. Institutional animal care and use committees and the challenges of evaluating animal research proposals. Res Integr peer Rev. 2025;10:11.

29. Matejkova N, Korecká L, Salek P, Kockova O, Pavlova E, Kasparova J, et al. Hyaluronic acid nanoparticles with parameters required for in vivo applications: from synthesis to parametrization. Biomacromolecules. 2024;25:4934–45.

30. Riglet L, Delgado T, Lopez RF, Pers Y-M, Cyteval C, Adam P, et al. Efficacy and safety of a combination of platelet-rich plasma with non-crosslinked hyaluronic acid versus a crosslinked hyaluronic acid, in single-injection for knee osteoarthritis. Randomized, controlled, multicenter, non-inferiority trial. BMC Musculoskelet Disord. 2026;27:272.

31. Marinescu E-A, Nica O, Ilinoiu E, Cojocaru A, Negrilă AA, Ciurea ME. PRP Enriched with Hyaluronic Acid-PRP from Rat Protocol and Method of Preparation. Curr Heal Sci J. 2021;47:42–8.

32. Castro KC de, Burga-Sánchez J, Nogueira Campos MG, Mei LHI. Water-based synthesis of photocrosslinked hyaluronic acid/polyvinyl alcohol membranes via electrospinning. RSC Adv. 2020;10:31271–9.

33. Dai W, Zeng M, Zhang L, Shi G, Wang H, Xu C, et al. A kneading-responsive hyaluronic acid-based hydrogel for on-demand local anesthesia in osteoarthritis. Acta Biomater. 2025.

34. Muñoz-Trejo CA, Chuc-Gamboa MG, Cauich-Rodríguez J V, Vargas-Coronado RF, Escobar-García DM, Pozos-Guillen A, et al. Oxidized Hyaluronic Acid-Based Sponges: A Promising Biomaterial for Oral Mucosa Lesion Application. Int J Mol Sci. 2025;26:10383.

35. Shimojo AAM, da Silva Santos Duarte A, Santos Duarte Lana JF, Cristina Malheiros Luzo Â, Fernandes AR, Sanchez-Lopez E, et al. Association of platelet-rich plasma and auto-crosslinked hyaluronic acid microparticles: Approach for orthopedic application. Polymers (Basel). 2019;11:1568.

36. Linjawi AI. Sealants and white spot lesions in orthodontics: a review. J Contemp Dent Pract. 2020;21:808–14.

37. Pinto AS, Alves LS, do Amaral Zenkner JE, Zanatta FB, Maltz M. Gingival enlargement in orthodontic patients: Effect of treatment duration. Am J Orthod Dentofac Orthop. 2017;152:477–82.

38. Abid MF, Alhuwaizi AF, Al-Attar AM. Do orthodontists aim to decrease the duration of fixed appliance treatment? J Orthod Sci. 2021;10:6.

39. Gonçalves A, Monteiro F, Brantuas S, Basset P, Estevez A, Silva FS, et al. Clinical

and preclinical evidence on the bioeffects and movement-related implications of photobiomodulation in the orthodontic tooth movement: A systematic review. Orthod Craniofac Res. 2025;28:12–53.

40. Danz JC, Degen M. Selective modulation of the bone remodeling regulatory system through orthodontic tooth movement—a review. Front Oral Heal. 2025;6:1472711.

41. Jiménez-Peña OM, Ríos-Osorio N, Velandia-Palacio LA, Gómez-Moreno G, Grajales M. Effectiveness of photobiomodulation with low-level lasers on the acceleration of orthodontic tooth movement: an umbrella review. Evid Based Dent. 2025;26:113–4.

42. Pilloni A, Shirakata Y, Marini L, Božić D, Miron RJ, Rotundo R, et al. Hyaluronic acid: A novel approach in regenerative/reconstructive periodontal therapy? Periodontol 2000. 2025.

43. Mansour A, Acharya AB, Alliot C, Eid N, Badran Z, Kareem Y, et al. Hyaluronic acid in Dentoalveolar regeneration: Biological rationale and clinical applications. J Oral Biol Craniofacial Res. 2024;14:230–5.

44. Zhu L, Li P, Qin Y, Xiao B, Li J, Xu W, et al. Platelet-rich plasma in orthopedics: bridging innovation and clinical applications for bone repair. J Orthop Surg. 2024;32:10225536231224952.

45. Chen J, Liu B, He J, Wei Y, He Y, Zhou H, et al. Multimodal mechanisms of platelet-rich plasma in bone defect repair: Angiogenesis, inflammation modulation, and metabolic regulation. Regen Ther. 2025;30:920–32.

46. Jaiswal A, Sennimalai K, Raghani MJ, Siddiqui HP, Galhotra V, Gandham R. Evaluating the efficacy of platelet-rich plasma on orthodontic tooth movement rate: a systematic review and meta-analysis. J World Fed Orthod. 2024;13:229–39.

47. Polizzi A, Leanza Y, Belmonte A, Grippaudo C, Leonardi R, Isola G. Impact of hyaluronic acid and other re-epithelializing agents in periodontal regeneration: A molecular perspective. Int J Mol Sci. 2024;25:12347.

48. Li Z, Zhou J, Chen S. The effectiveness of locally injected platelet-rich plasma on orthodontic tooth movement acceleration. Angle Orthod. 2021;91:391–8.

49. Zhang K, Liu F, Zeng Y, Qi Y, Zhao Y. Biphasic energy dependent effects of 650 nm diode laser photobiomodulation on orthodontic tooth movement and compression zone bone remodeling in vivo. BMC Oral Health. 2026;26:952.

50. Zong C, Van Dessel J, Vande Velde G, Willems G, Cadenas de Llano-Pérula M. Dynamic changes in tooth displacement and bone morphometry induced by orthodontic force. Sci Rep. 2022;12:13672.

51. Jeon HH, Teixeira H, Tsai A. Mechanistic insight into orthodontic tooth movement based on animal studies: a critical review. J Clin Med. 2021;10:1733.

52. Firth FA, Farrar R, Farella M. Investigating orthodontic tooth movement: challenges and future directions. J R Soc New Zeal. 2020;50:67–79.

Supplementary Files

This is a list of supplementary files associated with this preprint. Click to download.

- SupplementalDataTables.docx